The ionizing radiation from massive stars and its impact on H II regions: results from modern model atmospheres

S. Simón-Díaz[1,2]★ and G. Stasińska[1]

[1]*LUTH, Observatoire de Paris, CNRS, Université Paris Diderot; 5 Place Jules Janssen, 92190 Meudon, France*
[2]*Geneva Observatory, University of Geneva, 51 chemin des Maillettes, 1290 Sauverny, Switzerland*

ABSTRACT

We present a detailed comparison of the ionizing spectral energy distributions (SEDs) predicted by four modern stellar atmosphere codes, TLUSTY, CMFGEN, WM-*basic* and FASTWIND. We consider three sets of stellar parameters representing a late O-type dwarf (O9.5 V), a mid-O-type (O7 V) dwarf and an early O-type dwarf (O5.5 V). We explore two different possibilities for such a comparison, following what we called *evolutionary* and *observational* approaches: in the *evolutionary* approach, one compares the SEDs of stars defined by the same values of $T_{\rm eff}$ and $\log g$; in the *observational* approach, the models to be compared do not necessarily have the same $T_{\rm eff}$ and $\log g$, but produce similar H and He I-II optical lines. We find that there is a better agreement, in terms of $Q({\rm H}^0)$, the ratio $Q({\rm He}^0)/Q({\rm H}^0)$ and the shape of the SEDs predicted by the four codes in the spectral range between 13 and 30 eV, when models are compared following the *observational* approach. However, even in this case, large differences are found at higher energies.

We then discuss how the differences in the SEDs may affect the overall properties of surrounding nebulae in terms of temperature and ionization structure. We find that the effect over the nebular temperature is not larger than 300–350 K. Contrarily, the different SEDs produce significantly different nebular ionization structures. This will lead to important consequences on the establishment of the ionization correction factors that are used in the abundance determination of H II regions, as well as in the characterization of the ionizing stellar population from nebular line ratios.

Key words: stars: atmospheres – stars: early-type – stars: fundamental parameters – H II regions.

1 INTRODUCTION

The intense far ultraviolet (FUV) radiation emitted by early OB-type stars ionizes the interstellar medium, generating the so-called H II regions. These regions can be used to derive properties of the associated stellar population (e.g. initial mass function, star-forming rate and age), and other properties of the galactic region where these are located, such as chemical composition. However, since the properties of H II regions crucially depend on the ionizing spectral energy distribution (SED) of the massive star population, and this part of the stellar flux is generally inaccessible to direct observations, the predictions resulting from massive star atmosphere codes are a crucial ingredient.

The outer layers of blue luminous stars are characterized by strong non-local thermodynamic equilibrium (LTE) conditions, spherically extended geometries and the effect of hundreds of thousands of flux absorbing metal lines present in the FUV and ultraviolet (UV) spectral ranges (producing the so-called line-blanketing and line-blocking effects, as well as the development of radiatively driven stellar winds). All the above effects must be taken into account when modelling the atmospheres of these stars. An ideal model atmosphere code should consider all of these problems in a detailed manner; however, this would require an enormous computational effort. To avoid this, depending on the specific study one wants to treat, some of the physical processes can be relaxed without affecting the reliability of the model output.

In the last decades, a great effort has been devoted to the development of stellar atmosphere codes for hot massive stars. The advent of the new generation of non-LTE, line-blanketed model atmosphere codes, either plane-parallel (TLUSTY, Hubeny & Lanz 1995), or spherically expanded (FASTWIND, Santolaya-Rey, Puls & Herrero 1997; Puls et al. 2005; CMFGEN, Hillier & Miller 1998; WM-*basic*, Pauldrach, Hoffmann & Lennon 2001) is already a fact. While CMFGEN aims to be the most exact one (and hence, the most time consuming), the other three use specific approximations in

★E-mail: sergio.simon-diaz@obs.unige.ch; ssimon@iac.es

the calculation of the stellar atmosphere structure and of the SED, reducing then the computational time.

New generation stellar atmosphere models, including a more realistic description of the physical processes characterizing the stellar atmosphere, produce quite different ionizing SEDs than the previous plane-parallel, hydrostatic models (either LTE by Kurucz 1991, or non-LTE by, e.g., Mihalas & Auer 1970; Kunze, Kudritzki & Puls 1992 and Kunze 1994). Some notes on this, and on the consequences on the ionization structure of H II regions, can be found in Gabler et al. (1989), Najarro et al. (1996), Sellmaier et al. (1996), Rubin, Kunze & Yamamoto (1995), Rubin et al. (2007), Stasińska & Schaerer (1997), Schaerer (2000) and Martín-Hernández et al. (2002). Although the new predictions seem to go in the right direction (viz. Giveon et al. 2002; Morisset et al. 2004), non-negligible differences can still be found between the various stellar codes (see e.g. Mokiem et al. 2004; Martins, Schaerer & Hillier 2005; Puls et al. 2005).

In this paper, we explore in detail the differences between the predictions in the FUV from four modern stellar atmosphere codes (TLUSTY, CMFGEN, WM-*basic* and FASTWIND), and study their effects on H II regions spectra. In Section 2, we present a set of stellar atmospheres constructed specifically for this purpose, and show that two different approaches can be followed to compare the SEDs: the *evolutionary* approach, in which the same values of $T_{\rm eff}$ and $\log g$ are used for models computed with the various stellar atmosphere codes; and the *observational* approach, in which the models to be compared do not necessarily have the same $T_{\rm eff}$ and $\log g$, but produce similar H and He I-II optical lines. In Section 3, by using simple, *ab initio*, H II region models, we study how the differences in the SEDs may affect the overall properties of surrounding nebulae in terms of temperature, ionization structure and other astrophysical diagnostics. Finally, Section 4 summarizes the main results and presents some prospects.

2 COMPARISON OF IONIZING SEDS FROM VARIOUS STELLAR ATMOSPHERE CODES

For the reader unfamiliar with stellar atmosphere modelling, the main characteristics of the codes TLUSTY, CMFGEN, WM-*basic* and FASTWIND are presented in the appendix (accessible online only).

2.1 Choice of stellar atmosphere models

Table 1 summarizes the stellar atmosphere models used for our study. Initially, we considered three stars with a gravity $\log g = 4.0$ dex and effective temperature $T_{\rm eff} = 30\,000$, $35\,000$ and $40\,000$ K,[1] and computed CMFGEN, FASTWIND and WM-*basic* models for each pair $T_{\rm eff}$–$\log g$. In order to exclude from our study, the possibility that discrepancies found between the stellar atmosphere codes calculations could be due to differences in the considered stellar and wind parameters and/or stellar abundances, those models were calculated taking care of using exactly the same set of parameters and abundances.

As part of the initial set of models, three TLUSTY models, taken from the OSTAR2002 grid[2] by Lanz & Hubeny (2003), were also

---

[1] Following the spectral type-$T_{\rm eff}$ calibration by Martins et al. (2005), these models would approximately represent a late O-type (O9.5 V), a mid-O-type (O7 V) and an early O-type (O5.5 V) dwarf, respectively.

[2] See also http://nova.astro.umd.edu/.

Table 1. Summary of stellar atmosphere models used in this work (C, W, F and T labelling CMFGEN, WM-*basic*, FASTWIND and TLUSTY, respectively).

Models	$T_{\rm eff}$ (kK)	$\log g$ (dex)	R ($R_\odot$)	$\log \dot{M}$ ($M_\odot$ yr^{-1})	v_∞ (km s^{-1})
C1, W1, F1, T1[†]	30.0	4.0	7.0	−7.28	2000
C2, W2, F2, T2[†]	35.0	4.0	9.0	−7.12	2000
C3, W3, F3, T3[†]	40.0	4.0	10.0	−6.93	2400
F4	31.0	4.1	7.0	−7.28	2000
W4	31.0	4.0	7.0	−7.28	2000
T4	30.5	4.1	–	–	–
F5	36.0	3.9	9.0	−7.12	2000
W5	36.0	4.0	9.0	−7.12	2000
T5	35.5	4.1	–	–	–
F6	41.0	4.0	10.0	−6.93	2400

[†]R, $\dot{M}$, and v_∞ only for CMFGEN, WM-*basic* and FASTWIND models.

considered (those labelled as G30000g400v10, G35000g400v10 and G40000g400v10, respectively).

Finally, another set of FASTWIND, WM-*basic* and TLUSTY models, with slightly modified values for the effective temperatures and gravities, was also computed. This was necessary for the approach presented in Section 2.4.

In all the cases, the metallicity was considered to be solar (following the set of abundances derived by Grevesse & Sauval 1998), and a microturbulence $\xi_{\rm t} = 10$ km s^{-1} was assumed in the model calculations.

2.2 Methodology

Two different approaches were followed to compare the SEDs from the various stellar atmosphere codes. Basically, these are characterized by the methodology used to establish the stellar parameters ($T_{\rm eff}$, $\log g$ and $\log L$). We call them *evolutionary* and *observational* approaches.

In the *evolutionary approach*, the stellar parameters characterizing a star are fixed by the output of stellar evolutionary codes. This approach is mainly used by stellar population synthesis codes, such as STARBURST99 (Leitherer et al. 1999, see also Smith, Norris & Crowther 2002) or PEGASE (Fioc & Rocca-Volmerange 1999). In this case, for a given initial stellar mass and evolutionary time, a star is defined by the $T_{\rm eff}$, $\log g$ and $\log L$ predicted by the stellar evolution codes (e.g. Schaller et al. 1992; Meynet & Maeder 2000, 2005).

On the other hand, when spectroscopic and photometric observations of the star are available, the stellar parameters can be derived by means of what we call an *observational approach*. In this case, the stellar and wind parameters are determined by fitting appropriate stellar line features using stellar atmosphere models. This is a long established way to analyse O-type star spectra. The optical H and He I-II lines have been mainly used to determine the stellar $T_{\rm eff}$ and $\log g$ (viz. Herrero et al. 1992; Herrero, Puls & Najarro 2002; Repolust, Puls & Herrero 2004), though the UV spectra of these stars also provide valuable information about the physical properties of their winds, such as terminal wind velocities and mass-loss rates (see Kudritzki & Puls 2000). In addition, in the observational approach, the stellar luminosity is obtained from the stellar absolute visual magnitude ($M_{\rm v}$).

For a quantitative comparison of ionizing SEDs, we used the quantity Q_E, indicating the number of photons with energy greater than $E = h\nu$. If the emergent stellar flux is given by $H_\nu(\lambda)$, these
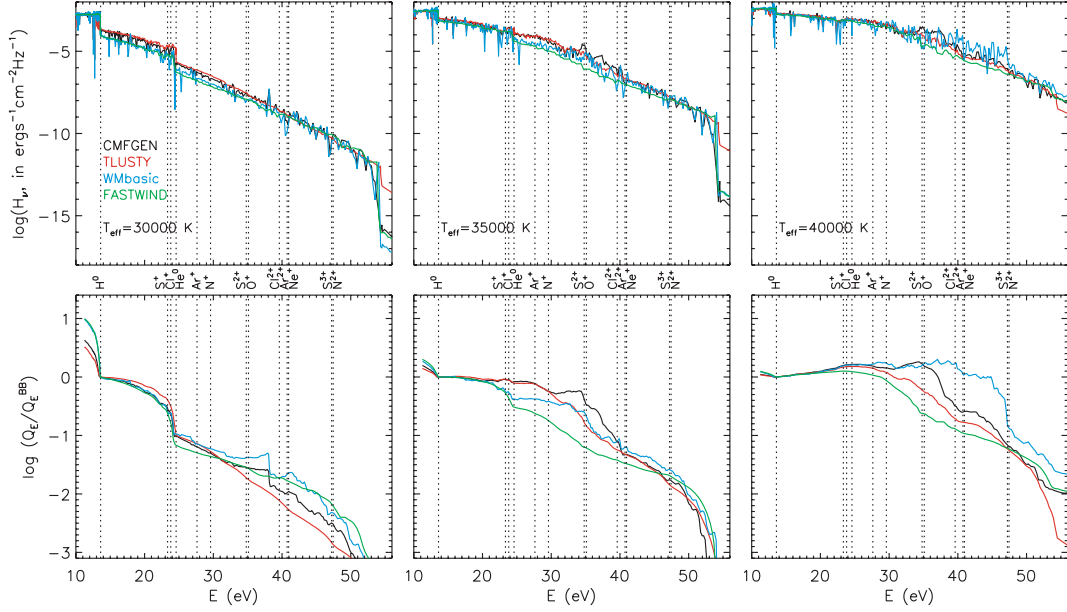
Figure 1. (Upper panels) Spectral energy distribution in the range 10–60 eV as predicted by the various stellar atmosphere codes. CMFGEN, TLUSTY, WM-*basic* and FASTWIND predictions are plotted as black, red, blue and green curves, respectively. The fluxes from WM-*basic*, CMFGEN and TLUSTY have been remapped to the FASTWIND frequency grid for a better comparison. (Lower panels) Comparison of the number Q_E of photons with energy greater than E relative to the corresponding number for a blackbody with $T = T_{eff}$. The location of the ionization edges of various ionic species of H, He, N, O, Ne, S, Cl and Ar with ionization energies below 54.4 eV (He^+ ionization energy) is also shown.

quantity is defined as follows

$$Q_E = \int_\nu^\infty \frac{L_\nu}{h\nu'} \, d\nu' = 16\pi^2 R^2 \int_0^\lambda \frac{H_\nu(\lambda')}{h\lambda'} \, d\lambda', \qquad (1)$$

where L_ν is the emergent stellar luminosity distribution and R is the stellar radius.

2.3 Comparison of SEDs in the evolutionary approach

In this section, we compare the SEDs resulting from CMFGEN, TLUSTY, WM-*basic* and FASTWIND when models with exactly the same stellar parameters are considered (T_{eff}, log g and L). Through this comparison, we can test the implications of using SEDs from the various stellar atmosphere codes as input for stellar population synthesis codes in order to compute photoionization models of giant H II regions.

Upper panels in Fig. 1 show the corresponding SEDs in the range 10–60 eV. This qualitative comparison already shows that the stellar atmosphere codes produce somewhat different ionizing SEDs. To quantify these differences, we first consider the total number of H^0 ionizing photons, and then compare the shape of the SEDs for energies $E > 13.6$ eV.

2.3.1 Ionizing luminosities

Table 2 summarizes the number of H^0 ionizing photons, $Q(H^0) = Q_{13.6}$, resulting from the various stellar atmosphere models. Note that in this case, the stellar radii (used in the calculation of the ionizing luminosities by means of equation 1) were fixed once a characteristic stellar luminosity was assumed for each effective temperature.

The values of log $Q(H^0)$ computed with the various codes for the same T_{eff}, log g, log L are found to differ significantly. In the worst case, i.e. between WM-*basic* and TLUSTY for $T_{eff} = 30\,000$, they differ

Table 2. Resulting number of H^0 ionizing photons (in logarithm) for the various stellar atmosphere codes when the same T_{eff} and log g are considered (*evolutionary* approach).

T_{eff}	30000	35000	40000
log g	4.0	4.0	4.0
log L	38.10	38.55	39.80
C1, C2, C3	47.33	48.39	48.99
T1, T2, T3	47.43	48.44	49.00
W1, W2, W3	46.97	48.30	48.93
F1, F2, F3	46.98	48.26	48.92

by ∼0.5 dex. The discrepancy tends to be lower for larger T_{eff}, but in the hottest star a difference of 0.08 dex (i.e. a factor of 1.2) can still be found between FASTWIND and CMFGEN models. Note, however, that there is always a good agreement (below 0.04 dex) between WM-*basic* and FASTWIND models on one hand, and CMFGEN and TLUSTY models on the other.

2.3.2 Shape of the ionizing SEDs

To study how the shape of the predicted SEDs compares in the H Lyman continuum,[3] we produced the diagrams shown in lower panels of Fig. 1. There we compare, for each energy E (eV), the number Q_E of photons with energy greater than E relative to the corresponding number for a blackbody with $T = T_{eff}$. Note that all spectra were scaled to have the same value for $Q_{13.6}$.

These diagrams can also be used to compare the number of ionizing photons for a certain ionic species, X^i, relative to the total

---

[3] Note that shocks were not considered in any of the models and consequently the emergent stellar flux in the X-ray domain is virtually zero.

number of hydrogen ionizing photons – $Q(X^i)/Q(H^0)$. This is the major factor determining the relative populations of different ions of a given element in an H II region, although its effect is modulated by the recombination and charge exchange coefficients.

Since we are interested on the impact that the ionizing radiation from massive stars has on H II regions, we only considered ions of those elements in which lines are commonly observed in H II regions (i.e. H, He, N, O, Ne, S, Cl and Ar). The corresponding ionization potentials are indicated as vertical lines in Fig. 1. Note that, for the range of effective temperatures we are considering, all the SEDs show an abrupt decrease in energies >54.4 eV. The effect of this part of the stellar flux on the ionization of the surrounding material in the case of H II regions is practically negligible, so we restrict our study to ions with ionization potential <54.4 eV.

Various conclusions concerning the shape of the SEDs can be emphasized from the inspection of Fig. 1.

(i) *30 000 K star.* In this case, FASTWIND and WM-*basic* models predict a larger H Lyman jump than the other two codes. This is consistent with the fact that a lower number of H^0 ionizing photons is resulting from FASTWIND and WM-*basic* models (see above).

Good agreement is found for all the codes except TLUSTY in the region between the H^0 and He^0 edges. This code is producing a somewhat harder flux, and hence larger $Q(S^+)$ and $Q(Cl^+)$ values.

While CMFGEN and WM-*basic* predict a similar He^0 jump, this break is larger in TLUSTY and FASTWIND SEDs. As a consequence, TLUSTY results in the same $Q(He^0)$ than FASTWIND and WM-*basic*, and FASTWIND in a smaller number of He^0 ionizing photons (~ 0.2 dex).

The slope of the SED above the He^0 edge is larger in TLUSTY and CMFGEN than in WM-*basic* and FASTWIND, which results in harder fluxes for these later codes for energies $E > 40$ eV.

It is also interesting to note how the presence of a strong emission line in 38 eV (present in WM-*basic* and CMFGEN spectra, but not in FASTWIND and TLUSTY) affects the resulting $Q(S^{2+})$ and $Q(O^+)$.

(ii) *35 000 K star.* The agreement between TLUSTY and CMFGEN is quite good, with discrepancies not larger than 0.1 dex in Q_E, except in the range 30–40 eV. This is a region of the stellar flux where metal-line blocking is important, and differences in the way this is treated (e.g. the amount of metal lines included in the blocking calculation), or differences in the ionization degree of the elements producing this forest of lines can affect the amount of flux emerging from the star in this spectral range. The discrepancy found between CMFGEN and TLUSTY in this spectral range translates in $Q(S^{2+})$ and $Q(O^+)$ values differing by ~ 0.4 dex.

Important discrepancies are found between these two codes and WM-*basic* and FASTWIND in the spectral range where the S^+, Cl^+, He^0, Ar^+ and N^+ ionizing edges are located (~ 23–30 eV). Both WM-*basic* and FASTWIND result in lower fluxes in this spectral range. For example, $Q(He^0)/Q(H^0)$ is ~ 0.3–0.4 dex smaller in FASTWIND and WM-*basic* than in the other codes. In addition, while WM-*basic* is closer to CMFGEN and TLUSTY for larger energies, FASTWIND is producing a lower flux between 30 and 45 eV.

In this case, WM-*basic* and FASTWIND are also resulting is a somewhat larger H Lyman edge (again consistent with results in Table 2).

(iii) *40 000 K star.* Good agreement is found between CMFGEN and TLUSTY (again except in the range 30–40 eV). FASTWIND predicts a somewhat lower flux than these two codes for $E \geq 25$ eV. On the other hand, while WM-*basic* results in a similar SED as CMFGEN for $E \leq 35$ eV, differences of up to 0.8 dex in Q_E are found for larger energies.

2.4 Comparison of SEDs in the observational approach

In this section, we check if the various stellar atmosphere codes are producing similar results for the lines normally used to estimate the stellar parameters. Then, we compare the SEDs given by models which do not have necessarily the same T_{eff} and $\log g$ but produce similar results for those lines.

2.4.1 Predicted stellar H and He optical lines

Fig. 2 shows the comparison of a representative set of H Balmer and He I–II synthetic lines for the various values of (T_{eff}, $\log g$), as predicted by FASTWIND, CMFGEN and TLUSTY. We decided to present results in two He I lines to account for the singlet-triplet problem
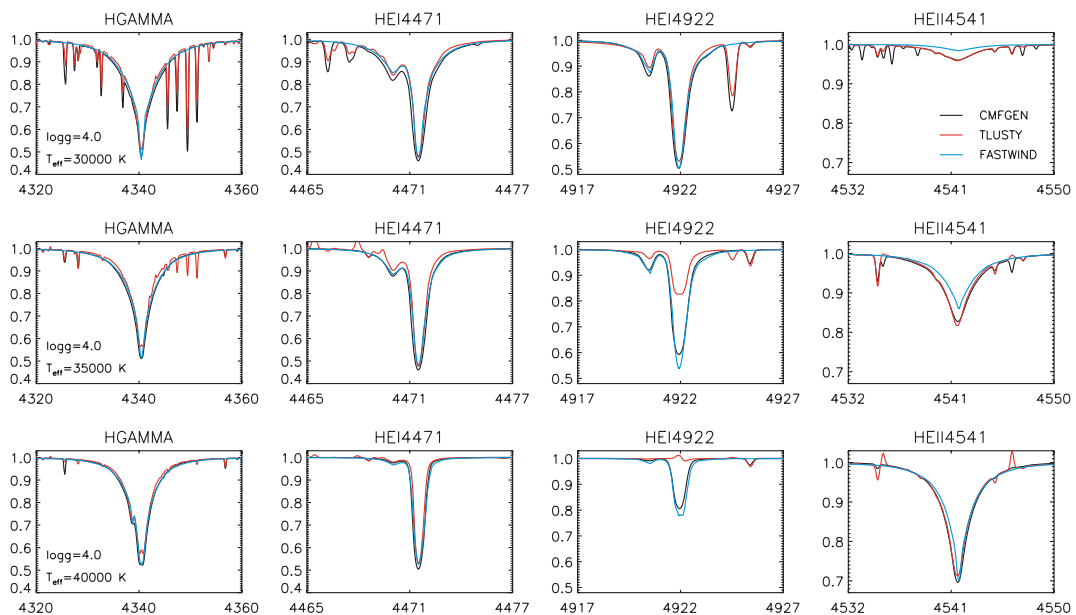

Figure 2. Comparison of some of the optical H, He I and He II lines commonly used to derive stellar parameters in O-type stars resulting from CMFGEN, TLUSTY and FASTWIND models. Note that only H and He lines are present in the FASTWIND synthetic spectra (see appendix).

Table 3. Stellar parameters ($T_{\rm eff}$ and $\log g$) required to fit FASTWIND and TLUSTY optical H and He lines to those resulting from CMFGEN models with $\log g = 4.0$ and $T_{\rm eff} = 30\,000$, 35 000 and 40 000 K, respectively. The labels indicated in brackets are the same as those used in Table 1.

CMFGEN	FASTWIND	TLUSTY
30000, 4.0 (C1)	31000, 4.1 (F4)	30500, 4.1 (T4)
35000, 4.0 (C2)	36000, 3.9 (F5)	35500, 4.1 (T5)
40000, 4.0 (C3)	41000, 4.0 (F6)	40000, 4.0 (T3)

Table 4. Number of H^0 ionizing photons for CMFGEN, TLUSTY, FASTWIND and WM-*basic* models with different stellar parameters ($T_{\rm eff}$ and $\log g$), but similar H and He optical lines. The stellar radius was determined following Kudritzki (1980), once an absolute visual magnitude ($M_{\rm v}$) was assumed for each set of models.

	$T_{\rm eff}$, $\log g$	V	$R/R_\odot$	$\log L$	$M/M_\odot$	$\log Q(H^0)$
			$M_{\rm v} = -3.5$			
C1	30000, 4.0	−29.09	6.3	38.05	14.3	47.28
T4	30500, 4.1	−29.09	6.2	38.07	17.8	47.45
F4	31000, 4.1	−29.05	6.3	38.11	18.5	47.40
			$M_{\rm v} = -4.3$			
C2	35000, 4.0	−29.37	7.9	38.52	22.8	48.36
T5	35500, 4.1	−29.37	7.9	38.54	28.8	48.45
F5	36000, 3.9	−29.37	7.9	38.57	18.2	48.40
			$M_{\rm v} = -4.8$			
C3	40000, 4.0	−29.55	9.2	38.88	31.0	48.97
T3	40000, 4.0	−29.52	9.3	38.89	31.8	49.00
F6	41000, 4.0	−29.56	9.2	38.92	30.6	48.99

(see Najarro et al. 2006, and references therein). WM-*basic* is not included in this comparison since the optical H and He I–II lines are not synthesized by this code.

While FASTWIND and CMFGEN produce quite similar H_γ wings (which are the main diagnostic to determine $\log g$), TLUSTY models would need a larger $\log g$ to produce the same result. On the other hand, while the three codes predict coherent results for the He I λ 4471 (triplet) line, this is not the case for the other He I λ 4922 (singlet) line. The cause of this discrepancy was already pointed out by Najarro et al. (2006), who also suggested that the He I triplet lines should be preferred in the spectral analysis due to the sensitivity of the He I singlet transitions to model assumptions. Finally, CMFGEN and TLUSTY agree almost perfectly regarding the He II λ 4541 line, while FASTWIND models result in a shallower line in the $T_{\rm eff} = 30\,000$ and 35 000 K cases. Although it is not shown here, a similar behaviour is also found for the other He II lines.

The above-mentioned result implies[4] that the codes are resulting in a somewhat different temperature and density structure in the stellar atmosphere, which in turn affect the strength of the He II lines (via the He ionization degree in the line formation region) and the wings of the H Balmer lines. On the other hand, the stellar parameters that would be derived from the spectroscopic analysis of a given observed spectrum are model dependent. To explore the differences in the stellar parameters that would be obtained when using the various codes, we obtained the $T_{\rm eff}$ and $\log g$ values required by FASTWIND and TLUSTY to produce similar optical H and He I–II than CMFGEN models, taken as reference. These are indicated in Table 3.

The discrepancies between the three codes for the 30 000 and 35 000 K stars are $\sim$500–1000 K in $T_{\rm eff}$ and 0.1 dex in $\log g$. Note that these discrepancies are of the same order as the accuracy reached when analysing *observed* spectra of OB-type stars with a given code ($\sim$1000 K in $T_{\rm eff}$ and 0.1 dex in $\log g$ – see e.g. Herrero et al. 2002; Repolust et al. 2004; Simón-Díaz et al. 2006). On the other hand, the agreement for the 40000 K star case is almost perfect.

In the next sections, we take into account these differences for the comparison of ionizing SEDs.

2.4.2 Ionizing luminosities

Table 4 indicates the number of H^0 ionizing photons for the models summarized in Table 3. The synthetic V magnitudes resulting from the models, along with the derived stellar radii, luminosities and masses are also indicated. Note that in this case, the stellar radii

were determined following Kudritzki (1980) once an absolute visual magnitude ($M_{\rm v}$) was assumed for each set of models.

In all cases, the agreement between models which result in similar H and He I–II lines is better than when the same stellar parameters are used to construct the models (see Table 2). Note, however, that differences up to 0.1 dex still remain. These differences are partially due to the somewhat different stellar radii (which are a consequence of the synthetic V magnitude resulting from the stellar models).

2.4.3 Shape of the ionizing SEDs

Fig. 3 compares the shape of the SEDs for those CMFGEN, TLUSTY and FASTWIND models resulting in similar H and He I–II lines.

In all the cases, the discrepancies found in the spectral range 13.6–30 eV when models with the same stellar parameters were compared (see Section 2.3 and Fig. 1) have practically disappeared. This is especially notable in the 35 000 K star case. In addition, the agreement between the three codes for the H Lyman break is quite good.

Although WM-*basic* could not be included in the comparison presented in Section 2.4.1 (since the optical H and He I–II lines are not synthesized by this code), in view of the above-mentioned results, we decided to also include the SED of those WM-*basic* models which, having an effective temperature and gravity close to those of CMFGEN models, produce similar SEDs as the other codes in the range 13.6–30 eV. These models correspond to those labelled W4, W5 and W3 in Table 1.

In general, the situation for higher energies has also improved; however, some important discrepancies still remain. From inspection of Fig. 3, it can be remarked as follows.

(i) FASTWIND gives much harder SEDs than the other codes in the 30 000 K case.

(ii) WM-*basic* results in harder fluxes than the other codes in the 35 000 and 40 000 K cases (this discrepancy is especially notable in the hottest star).

(iii) TLUSTY and CMFGEN SEDs agree quite well, except in the range 30–40 eV. In this energy range, the FASTWIND SED is closer to that of TLUSTY.

---

[4] Villamariz & Herrero (2000) showed that, except for He II λ 4686, the He II lines are practically insensitive to the adopted value of microturbulence. Note also that for effective temperatures in the range between 30 000 and 35 000 K, the sensitivity of the He I lines on $T_{\rm eff}$ is quite small.

Figure 3. As lower panels of Fig. 1 but for the CMFGEN, TLUSTY and FASTWIND models resulting in similar optical H and He I–II lines (see Section 2.4). The WM-*basic* models appearing in these plots were selected to produce similar SEDs as the other codes in the range 13.6–30 eV (see explanation in Section 2.5).

As commented by Puls et al. (2005), the number of metal lines between 35 and 50 eV is quite large, and the treatment of the opacities of the weakest lines affects the SED above 24.6 eV. The different approaches of the line-blanketing and wind effects might also contribute to the observed discrepancies. In addition, the fact that different effective temperatures are being considered in the various codes may affect the slope of the SED in the high-energy range.

2.5 The importance of the H and He line analysis in the comparison of SEDs

In the previous section, we have shown that the number of H^0 ionizing photons, the ratio $Q(He^0)/Q(H^0)$ and the shape of the SEDs below 30 eV agree better in the observational approach than in the evolutionary approach. This results from the fact that the shape of the emergent flux is a consequence of the stellar atmospheric structure (which, for a given set of stellar parameters, is influenced by the line- and wind-blanketing effects) and the blocking by numerous metal lines present in the FUV spectral range. Specifically, the size of H^0 and He^0 jumps is a function of the population of the ground levels of the corresponding ions in the respective continuum-forming regions. Temperature and electron density mainly control the level population of those ground levels (though wind effects can also contribute, see Gabler et al. 1989; Najarro et al. 1996). For example, in a star with larger effective temperature or lower gravity, H and He are expected to be more ionized in the corresponding continuum-forming regions, and hence the ground level population of H^0 and He^0 will be smaller, resulting in smaller H and He I jumps.

On the other hand, the optical H and He I–II lines depend mainly on the recombination from the corresponding upper ions (i.e. H^+, He^+ and He^{2+}, respectively) which, in turn, is controlled by temperature and electron density, again in the region of the stellar atmosphere where these transitions become optically thin. These line formation regions are normally located close to the regions where the H^0 and He^0 continua are formed, except maybe for H_α, He II λ 4686, He I λ 5875, the strongest lines.

By fitting the optical H and He I–II lines, one is fixing the physical properties (density and temperature) in the corresponding line-forming region, and hence in the H^0 and He^0 continuum-forming regions. Consequently, differences in the predicted SEDs, in terms of H^0 Lyman jump and $Q(He^0)/Q(H^0)$ ratio, and differences in the optical H and He II lines between any couple of models are strongly related.

Therefore, the study of the optical H and He I–II stellar lines provide very useful additional information to understand the possible discrepancies in the ionizing stellar SEDs predicted by the various stellar atmosphere codes.

2.6 Use of SpT–T_{eff} calibrations

In Section 2.2, we have presented two different approaches to establish the stellar parameters characterizing a star. There is still another way, based on SpT–T_{eff} calibrations.

It is important to note that while the spectral classification of a star provides a qualitative description of the stellar characteristics, and does not depend on any model calculation, the stellar parameters determination is dependent on the physics used in the stellar atmosphere modelling. For example, in the last years there has been an important revision of the calibrations of stellar parameters of O-type stars (see e.g. Martins et al. 2005). The inclusion of non-LTE, line-blanketing and wind effects in the stellar atmosphere code calculations resulted in SpT–T_{eff} calibrations indicating a lower effective temperature for a given spectral type compared to previous calibrations (Vacca, Garmany & Shull 1996).

The above results (Section 2.4) alert us that one must use the SpT–T_{eff} calibrations with care, because these are model dependent. Obviously, this does not mean that calibrations cannot be used at all, but it is important to understand that applying a calibration obtained with one code to create a grid of stellar SEDs for O-type stars with a different code would be an inconsistent way of doing. Moreover, even using the same code, it should be reminded that a certain dispersion is always associated with a given calibration. We refer the reader to Martins et al. (2005) and Mokiem et al. (2004) for a detailed discussion on the dependence of the SpT–T_{eff} calibrations on model assumptions such as microturbulence, metallicity and atmospheric and wind parameters. As commented by Martins et al. (2005), their theoretical T_{eff} scale should be taken as indicative since it is expected to have an uncertainty of ±1000 to 2000 K due to both a natural dispersion and uncertainties inherent to the methodology they applied.

3 PREDICTED EFFECTS OF DIFFERENT SEDS ON SURROUNDING NEBULAE

In this section, we investigate how the differences in the SEDs may affect the overall properties of surrounding ionized nebulae. For illustrative purposes, we have constructed a set of *ab initio*

photoionization models with CLOUDY,[5] using as an input the SEDs from the stellar atmosphere models discussed above.

To isolate the dependence of the nebular ionization structure on the stellar SED from the other factors that may also affect it, such as nebular gas distribution and ionization parameter, we limited ourselves to spherical constant density models ($N_H = 1000\,\mathrm{cm^{-3}}$, $R_{int} = 10^{15}\,\mathrm{cm}$), and the same $Q(\mathrm{H}^0)$ was considered for each set of stellar parameters. The adopted nebular abundances were those of the Orion nebula and all the models are dust-free.

3.1 Effect on the nebular temperature

3.1.1 General considerations

At each pointing the nebula, the electron temperature, T_e, is the result of balance between heating and cooling processes. The energy gains in a photoionized nebula are usually dominated by photoionization of hydrogen atoms, with some contribution of photoionization of helium (Osterbrock 1989; see also review by Stasińska 2004). It can be shown that, when ionization equilibrium is achieved, the energy gains due to ionization of H^0 and He^0 can, in a first approximation, be written as

$$G = n_H^+ n_e \left(\langle E_H \rangle \alpha_H + \langle E_{He} \rangle \alpha_{He} \frac{n_{He}}{n_H} \frac{n_{He}^+}{n_{He}} \frac{n_H}{n_H^+} \right), \qquad (2)$$

where $\langle E_H \rangle$ is the average energy gained per photoionization of an H^0 atom:

$$\langle E_H \rangle = \frac{\int_{h\nu_0}^{\infty} 4\pi \frac{J_\nu(r)}{h\nu} e^{-\tau_\nu(r)} a_\nu(\mathrm{H}^0)(h\nu - h\nu_0)\mathrm{d}h\nu}{\int_{h\nu_0}^{\infty} 4\pi \frac{J_\nu(r)}{h\nu} e^{-\tau_\nu(r)} a_\nu(H^0)\,\mathrm{d}h\nu}, \qquad (3)$$

with J_ν being the intensity of the ionizing radiation. An expression similar to equation (3) can be written for $\langle E_{He} \rangle$.

Therefore, $\langle E \rangle$ depends on the shape of the ionizing SED, but not on the stellar luminosity, nor on the distance to the ionizing source.

On the other hand, the most important source of cooling in the nebula is generally collisional excitation of low lying energy levels of abundant elements (O, S, N) followed by radiative de-excitation.

3.1.2 Quantitative effects of different SEDs on T_e

Table 5 summarizes various nebular temperature averages (over volume and weighted by the electron density) predicted by CLOUDY models using the SEDs from the stellar models considered in Section 2.3.

The first thing that can be noted is that, in spite of the large differences found between some of the SEDs (see Fig. 1), the resulting nebular electron temperatures do not differ by more than 300–350 K.

To understand this, one should note that in the calculation of $\langle E \rangle$ from equation (3), the shape of the stellar SED is modified by the effect of absorption of stellar radiation in intervening nebular layers, $e^{-\tau_\nu}$, and by the absorption cross-section, $a_\nu(\mathrm{H}^0)$. Therefore, the contribution of different spectral regions from the SED to the nebular heating is not equally important. The functions to be integrated in the numerator of equation (3), for the case of an optical thickness of zero,[6] are plotted in Fig. 4, with the left-hand panels corresponding to H and the right-hand panels corresponding to He. FASTWIND

---

[5] We used version 07.02 of CLOUDY, last described by Ferland et al. (1998).
[6] Inside the nebula, those functions are affected by absorption, and by the contribution of the diffuse ionizing radiation produced in the nebula, both of which are dependent on the SED only to second order.

Table 5. Nebular temperature averages (over volume) weighted by the electron density predicted by CLOUDY models using the SEDs from the stellar models considered in Section 2.3.

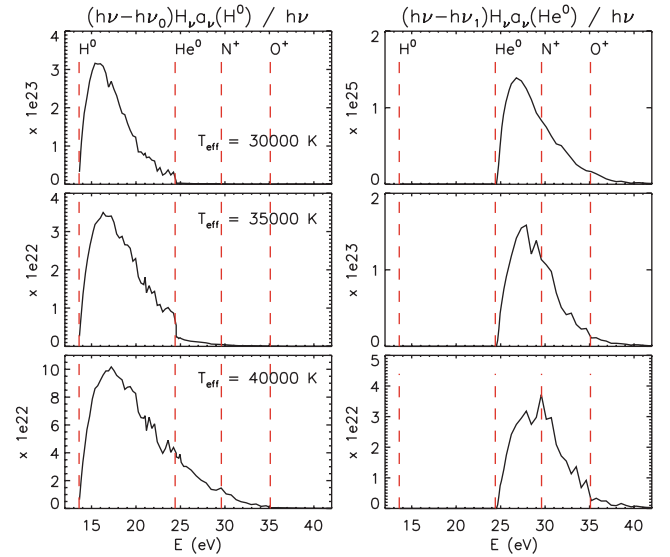|	T_e	$T_e(\mathrm{O}^{2+})$	$T_e(\mathrm{O}^+)$
C1	7100	6960	7100
T1	7340	7240	7340
W1	7060	6890	7070
F1	7040	6910	7040
C2	7580	7410	7760
T2	7820	7670	7930
W2	7630	7480	7730
F2	7750	7630	7790
C3	8280	8170	9100
T3	8340	8200	8880
W3	8190	8070	8960
F3	8360	8170	8690

Figure 4. Numerator functions to be integrated to calculate $\langle E_H \rangle$ (left-hand panel) and $\langle E_{He} \rangle$ (right-hand panel) from equation (3). Note the different scales used in each plot.

stellar SEDs for stars with $T_{eff} = 30\,000$, $35\,000$ and $40\,000$ K (from top to bottom, respectively) were used as illustrative. These figures show that the average energy gained per photoionization of H^0 in the nebula is independent of the SED above 25 eV for the stars with $T_{eff} = 30\,000$ and $35\,000$ K, and 35 eV for the $T_{eff} = 40\,000$ K case. Consequently, if the SEDs predicted by the stellar atmosphere codes differ below these energy limits, the nebular electronic temperature may be different. On the other hand, differences in the SEDs above these limits will not have any effect on the heating of the nebular gas. A similar argument can be applied to the heating by photoionization of He^0, which is dominated by photons with energies around 30 eV. Note, however, that the latter is always much smaller than H^0 heating, because of the n_{He}/n_H factor in equation (2).

One could then expect that, for a photoionization model with the same nebular abundances, the harder the ionizing fluxes for energies between 15 and 30 eV, the higher the nebular electron temperature. However, from inspection of the first column of Table 5, it can be

seen that actually this is not the general behaviour. For example, in the $T_{eff} = 35\,000$ K case, while CMFGEN is resulting in the hardest ionizing flux (see Fig. 1), the corresponding photoionization model is the one giving the lowest T_e. On the other hand, for the same star case, in spite of the fact that CMFGEN and TLUSTY are producing a similar heating, there is a difference in T_e between the associated CLOUDY models of 240 K.

The reason for this is that, although the nebular abundances are the same, the various SEDs are producing a different nebular ionization structure and hence the ionic fractions of O^{2+}, O^+, S^{3+}, S^{2+}, S^+ and N^+ (main coolants) are different. For example, in the first case mentioned above, since the number of O^+ ionizing photons is larger in CMFGEN (see Fig. 1), the population of O^{++} will be larger in the nebula. Since [O III] optical and infrared (IR) lines are very efficient coolants, the overall cooling will be more effective. Note that this effect is so strong that the resulting nebular T_e in the O^{2+} region (and hence in the global nebula) is lower than for the nebula ionized by FASTWIND model, which has a weaker ionizing flux, but the amount of O^+ ionizing photons is smaller.

Because of this effect, the shape of the SED in the spectral range containing the O^+ and S^{2+} edges is crucial. This range is precisely where the larger dispersion between the various SEDs is found, even when the fluxes are compared in the *observational* approach (see Fig. 3).

Obviously, the magnitude of these effects depends on the star and on the nebula under consideration. For example, in the $T_{eff} = 30\,000$ K case, the O^{2+} region is very small, and hence the global effect of cooling by [O III] lines is not very important. In this case, both $T_e(O^+)$ and T_e are similar, and the nebula with a higher T_e is the one ionized by TLUSTY, whose stellar flux is the hardest in the 20–25 eV region.

Fig. 5 illustrates the effect of the various SEDs on the nebular temperature from a different point of view. Here, we plot the values of the T_e indicators [S III] 6312/[S III] 9532 (left-hand panel) and [N II] 5755/[N II] 6584 (right-hand panel) as would be measured through a small square slit as a function of the projected distance to the central star, i.e. after integrating the line emissivities along a chord through the spherical H II region. Following the same set of colors used along the paper, models using SEDs from CMFGEN, TLUSTY, WM-*basic* and FASTWIND are represented in black, red, blue and green lines, respectively. The electron temperatures that would be derived from a given T_e indicator differ by about 200–300 K at most.

3.2 Effect on the nebular ionization structure

Contrary to the energy gains, which result from an integration over energy of the ionizing photons, the nebular ionization structure depends on the *details* of the SED. One can thus suspect that differences in the SEDs obtained with various stellar atmosphere codes will translate into significant differences in the ionization structures of the nebulae.

3.2.1 General considerations

The state of ionization of a nebula depends only, in first approximation, on the ionization parameter, U, and on the hardness of the ionizing radiation. Following Vilchez & Pagel (1988),

$$\frac{n(X^{i+1})}{n(X^i)} \propto U \frac{\int_{\nu(X^i)}^{\infty} \frac{H_\nu}{h\nu} \, \mathrm{d}\nu}{\int_{13.6\,\mathrm{eV}}^{\infty} \frac{H_\nu}{h\nu} \, \mathrm{d}\nu} \propto U \frac{Q(X^i)}{Q(H^0)}, \tag{4}$$
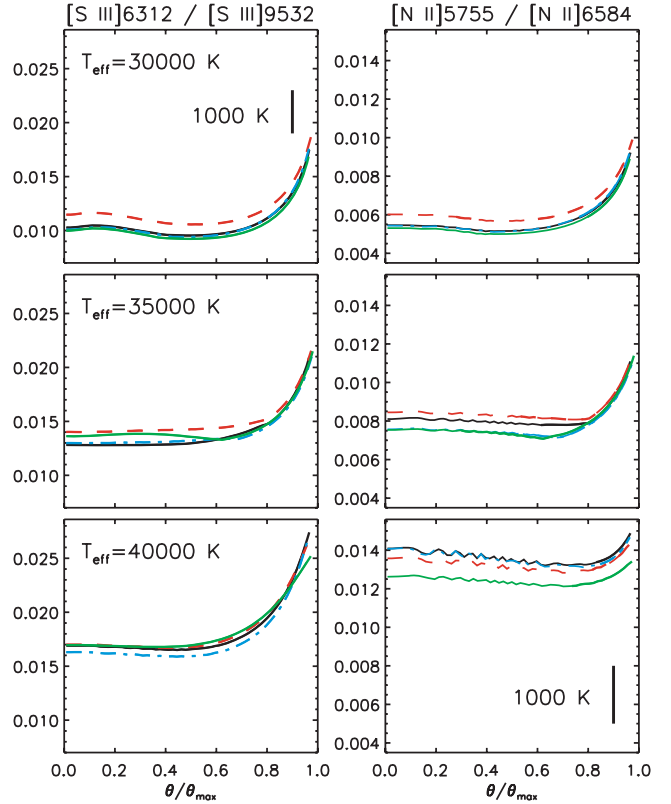

Figure 5. Nebular T_e diagnostic line ratios from the *ab initio* photoionization models. Models using SEDs from CMFGEN, TLUSTY, WM-*basic* and FASTWIND are plotted as black, red, blue and green curves, respectively. The vertical lines show the effect a variation of 1000 K in the electron temperature on the line ratios.

where $n(X^i)$ is the number density of the i times ionized atoms of element X, and H_ν is the stellar Eddington flux. Therefore, a ratio $n(X^{i+1})/n(X^i)$ is, to a first order and for a given U, proportional to the relative number of photons able to ionize X^i, as compared to that of Lyman continuum photons. Note, however, that photoionization models show that equation (4) is not exactly fulfilled (Stasińska & Schaerer 1997) rendering the interpretation more complex. Indeed, equation (4) ignores the effect of the modification of the radiation field in the nebula due to nebular emission and absorption.

3.2.2 Quantitative effects on the nebular ionization structure

Table 6 summarizes the predictions resulting from CLOUDY models using the stellar SED from the various stellar atmosphere codes in terms of the ionic fractions (in logarithm) for several elements. A comparison of these quantities can give us an idea of the effect that differences in the stellar SEDs are producing on the nebular ionization structure. As expected, in some cases photoionization models are resulting in enormous differences in these values for these quantities (up to ~1 dex for some cases). Obviously, there is a direct relation between how these quantities compare and the discrepancies found in Fig. 1 for the stellar ionizing SEDs. For example, the largest difference in the ratio $Q(He^0)/Q(H^0)$ was found between FASTWIND and CMFGEN for the 35 000 K star case (~0.4 dex) and, consequently, the largest difference in the ratio

Table 6. Integrated ionic ratios (in logarithm) predicted by CLOUDY photoionization models using the SEDs from the stellar models considered in Section 2.3.

	He^+/H^+	O^{2+}/O^+	Ne^{2+}/Ne^+	S^{3+}/S^{2+}	Ar^{2+}/Ar^+
C1	−2.163	−2.535	−3.599	−4.059	−1.249
T1	−2.130	−2.663	−3.842	−4.235	−1.209
W1	−2.087	−2.368	−3.263	−3.869	−1.166
F1	−2.205	−2.561	−3.415	−4.040	−1.303
C2	−1.293	−0.618	−1.775	−1.906	−0.020
T2	−1.311	−0.885	−1.814	−2.291	−0.058
W2	−1.531	−0.932	−1.777	−2.224	−0.418
F2	−1.639	−1.346	−2.079	−2.796	−0.573
C3	−1.012	0.531	−0.375	−0.777	1.528
T3	−1.016	0.173	−0.587	−1.166	1.379
W3	−1.012	0.506	0.144	−0.799	1.493
F3	−1.047	−0.173	−0.838	−1.537	0.899

Table 7. Results for the N^+/O^+ and Ne^{2+}/O^{2+} ionic ratios predicted by CLOUDY photoionization models using the SEDs from the stellar models considered in Section 2.3.

	$(N^+/O^+)/(N/O)$	$(Ne^{2+}/O^{2+})/(Ne/O)$
C1	1.002	0.086
T1	1.000	0.066
W1	0.998	0.127
F1	1.002	0.139
C2	0.804	0.085
T2	0.748	0.132
W2	0.899	0.157
F2	0.910	0.192
C3	0.668	0.385
T3	0.445	0.345
W3	0.612	0.767
F3	0.422	0.317

He^+/H^+ predicted by the photoionization models is also found for the same case (0.35 dex difference).

The fact that different SEDs produce different ionization structures has important consequences on abundance determinations and on the evaluation of the mean effective temperature of the ionizing stars.

(i) *Effects on ionic ratios*. In Table 7, we consider the nebular ratios N^+/O^+ and Ne^{2+}/O^{2+}. A common way to derive N abundances in H II regions is to use [N II] and [O II] lines, and correct for the unseen N^{2+} assuming that: $N/O = N^+/O^+$. Similarly, the Ne abundance is obtained assuming that $Ne/O = Ne^{2+}/O^{2+}$. Both formulae are recipes based on similarities of ionization potentials. Table 7 shows that not only these formulae are necessarily correct, but also that the value of these ratios depends on the considered SEDs, even the ionization potentials of N^+ and O^+ are so close to each other (as seen in Fig. 1).

(ii) *Estimation of the mean temperature of the ionizing stars*. This can be done by considering line ratios arising from different ions of the same element. The most popular indicator is the radiation softness parameter $\eta = (O^+/O^{2+})/(S^+/S^{2+})$ proposed by Vilchez & Pagel (1988). A better way to estimate the hardness of the ionizing radiation field is to plot the observational points in the $\eta(S–Ne) = ([S\ IV]/[S\ III])/([Ne\ III]/[Ne\ II])$ versus [Ne III]/[Ne II] plane, as shown by Morisset (2004). $\langle T_{eff} \rangle$ is then derived, together with

the ionization parameter U, by comparison with grids of models. In Fig. 6, we show the position of the compact H II region G29.96−0.02 (Morisset et al. 2002) with respect to small grids of models constructed with each of the four stellar atmosphere codes under study. In this case, we have excluded the 30 000 K star case and consider stellar models[7] with $T_{eff} = 45\,000$ K and log $g = 4.0$ dex. We see that, while CMFGEN and TLUSTY would infer $\langle T_{eff} \rangle \simeq 40\,000$ K, WM-*basic* would imply $\langle T_{eff} \rangle \sim 37\,000$ K and FASTWIND would give $\langle T_{eff} \rangle \sim 38\,500$ K.

The differences between the values of $\langle T_{eff} \rangle$ obtained using different codes are due not only to the difference in the general slopes of the SEDs, but also to local properties of the SEDs close to the ionization potentials of the involved ions.

If diagrams like those of Fig. 6 are used to simply order the values of $\langle T_{eff} \rangle$ of a sample of H II regions, one will probably obtain roughly the same ordering whatever atmosphere code is used (provided that one uses a diagram of appropriate metallicity for each object $\langle T_{eff} \rangle$, as described by Morisset 2004). But, as Fig. 6 shows, taking as granted the absolute values of $\langle T_{eff} \rangle$ are risky, since it depends so much on the stellar atmospheres used to determine them.

An additional problem is that the results depend strongly on whether the diagrams are constructed using models of dwarf stars or supergiants. In general, for a given T_{eff} the ionizing SED is harder in a star with lower gravity; therefore, lower stellar temperatures will be derived if based on models of supergiants. This is the reason why we obtained a larger $\langle T_{eff} \rangle$ for the ionizing star of G29.96−0.02 than Morisset et al. (2002), since they used stellar models with lower gravities.

4 SUMMARY

The aim of this paper was to study how various modern stellar atmosphere codes compare in terms of ionizing SEDs and how this affects the emission-line spectra of surrounding nebulae. This is important, since different codes predict quite different ionizing SEDs, which, in turn, impinges on the quantitative interpretation of H II regions spectra in terms of formation history, temperature of ionizing radiation or chemical composition.

We have computed models using four state-of-the-art stellar atmosphere codes: TLUSTY, CMFGEN, WM-*basic* and FASTWIND. All these codes account for non-LTE and line-blanketing effects, but with different emphasis on specific aspects. TLUSTY is a plane-parallel, hydrostatic code, while the other three belong to the family of models atmosphere codes so-called 'unified models'. On the other hand, while TLUSTY and CMFGEN consider a fully consistent treatment of line blanketing, WM-*basic* and FASTWIND use a fast numerical method to account for the line-blanketing and blocking effects. Three sets of stellar parameters representing a late O-type (O9.5 V), a mid-O-type (O7 V) and an early O-type (O5.5 V) dwarfs were considered, with the chemical composition and microturbulence being exactly the same in all models, so as to perfectly isolate the effects on physics and numerical prescriptions from the effect of secondary input parameters.

We have shown that, in order to compare the ionizing SEDs predicted by various stellar atmosphere codes, it is important to distinguish between what we called *evolutionary* and *observational* approaches. The *evolutionary* approach compares SEDs of stars defined by the same values of T_{eff} and log g, and is relevant for

---

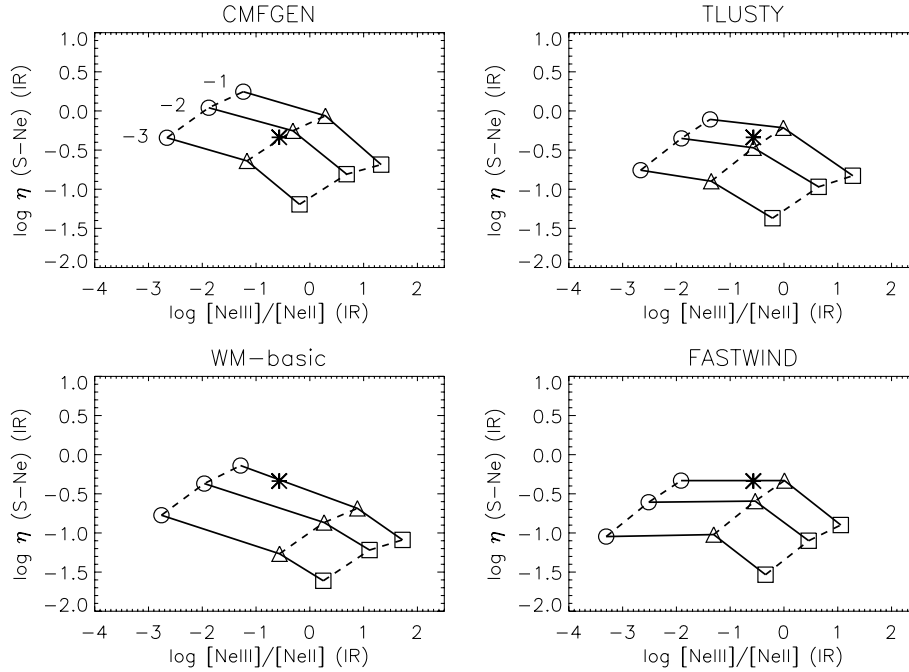[7] These models were computed following the same ideas as those presented in Section 2.1.

Figure 6. Diagnostic diagrams proposed by Morisset et al. (2004) to derive $\langle T_{eff} \rangle$ and U by comparing nebular IR data with results from grids of photoionization models. The corresponding IR lines used for the diagrams are [S IV] 10.5, [S III] 18.7, [Ne III] 15.5 and [Ne II] 12.8 μm. The figure shows the position of the compact H II region G29.96−0.02 studied by Morisset et al. (2002) with respect to small grids of models constructed with each of the four stellar atmosphere codes under study. The grids were constructed using photoionization models with $\log U = -3, -2, -1$ using fluxes from stellar models with $T_{eff} = 35, 40$ and 45 kK (circles, triangles and squares, respectively).

studies based on stellar population synthesis. On the other hand, it is the *observational* approach which is needed when using H II regions to probe theoretical SEDs. In this approach, the models to be compared do not necessarily have the same T_{eff} and $\log g$, but they produce similar intensities and profiles for the stellar H and He I–II lines normally used to estimate the stellar parameters. Note that a combined tailored modelling of a massive star and its surrounding ionized nebula would precisely use the *observational* approach.

We have shown that the study of the optical H and He I–II stellar lines helps understanding the origin of differences in the ionizing SEDs predicted by various stellar atmosphere codes. There is a better agreement – in terms of the total number of H ionizing photons $Q(H^0)$, of the ratio $Q(He^0)/Q(H^0)$, and of the shape of the SED in the spectral range 13–30 eV – between models resulting in similar H and He I–II lines than between models constructed with exactly the same T_{eff} and $\log g$. Therefore, to probe the ionizing radiation from massive stars by using nebular lines from surrounding H II regions,[8] it is important to secure high-quality spectra of the ionizing stars, allowing one to accurately determine the stellar parameters. Photoionization modelling will then permit one to investigate the ionizing SED above 30 eV (where the shape of the SED is known to be very sensitive to the treatment of line blocking, line-blanketing and stellar wind effects).

We then examined the emission-line spectra of *ab initio* models of H II regions constructed with the various atmosphere codes. We found that the nebular temperatures do not differ by more than 300–

350 K, and that the changes are not always in the direction expected from the change in the heating rate: differences in the cooling rate, induced by the modification of the ionization structure, also play a role. The ionization structure itself may change substantially. This has an impact on the abundance ratios derived from H II regions spectra, either by tailored photoionization modelling or with the help of ionization correction factors. For example, we have found that the values of N^+/O^+ and Ne^{2+}/O^{2+}, commonly identified with the N/O and Ne/O abundance ratios, may differ by 0.2–0.3 dex from one SED to another. The changes in the ionization structure also affect the temperature of the ionizing stars estimated from the emission-line ratios produced by the nebula. In the example, we considered the estimated T_{eff} varies from $\simeq 37\,000$ to $40\,000$ K.

Note that, in this paper, we presented models for dwarf stars only. For supergiant stars, the comparative behaviour of models obtained with the various codes may be different. For example, while Morisset et al. (2004) found that the difference between *wm-basic* and *cmfgen* models for supergiants with $T_{eff} = 40\,000$ K is positive in the >35 eV range, we found the opposite for dwarfs with the same T_{eff} (see also fig. 8 in Morisset et al. 2004). It is likely that the behaviour will change also with the chemical composition.

The problem is therefore complex and has to be analysed further. In any case, the limited study presented in this paper shows that, than even with the latest generation of stellar atmosphere codes, one must be careful when combining them with photoionization codes to establish the ionization correction factors to be used in the abundance determination of H II regions, or to characterize the ionizing stellar population from nebular line ratios.

The follow-up of this study will be to analyse in detail a few Galactic H II regions and their central stars, performing a combined stellar and nebular modelling, in order check which of the stellar

[8] Table B1 in Appendix B (accessible online only) indicates the available optical and IR nebular line ratios useful to test the predicted emergent ionizing SEDs.

atmosphere codes provide the best ionizing SED. Hopefully, this study and our forthcoming papers will have an impact on our understanding of the physics of stellar atmospheres, as well as on the reliability of the predictions from stellar synthesis codes and of abundance determinations in H ɪɪ regions.

ACKNOWLEDGMENTS

REFERENCES

Anderson L. S., 1989, BAAS, 21, 742
Bouret J.-C., Lanz T., Hillier D. J., Heap S. R., Hubeny I., Lennon D. J., Smith L. J., Evans C. J., 2003, ApJ, 595, 1182
Castor J. I., Abbott D. C., Klein R. I., 1975, ApJ, 195, 157
Esteban C., Peimbert M., García-Rojas J., Ruiz M. T., Peimbert A., Rodríguez M., 2004, MNRAS, 355, 229
Ferland G. J., Korista K. T., Verner D. A., Ferguson J. W., Kingdon J. B., Verner E. M., 1998, PASP, 110, 761
Fioc M., Rocca-Volmerange B., 1999, preprint (arXiv:astro-ph/9912179)
Gabler R., Gabler A., Kudritzki R. P., Puls J., Pauldrach A., 1989, A&A, 226, 162
Giveon U., Sternberg A., Lutz D., Feuchtgruber H., Pauldrach A. W. A., 2002, ApJ, 566, 880
Grevesse N., Sauval A. J., 1998, Space Sci. Rev., 85, 161
Herrero A., 2007, 704, preprint (arXiv:0704.3528)
Herrero A., Kudritzki R. P., Vilchez J. M., Kunze D., Butler K., Haser S., 1992, A&A, 261, 209
Herrero A., Puls J., Najarro F., 2002, A&A, 396, 949
Hillier D. J., Miller D. L., 1998, ApJ, 496, 407
Hubeny I., 1988, CoPhC, 52, 103
Hubeny I., Lanz T., 1992, A&A, 262, 501
Hubeny I., Lanz T., 1995, ApJ, 439, 875
Hubeny I., Hummer D. G., Lanz T., 1994, A&A, 282, 151
Jamet L., Stasińska G., Pérez E., González Delgado R. M., Vílchez J. M., 2005, A&A, 444, 723
Kudritzki R.-P., 1980, A&A, 85, 174
Kudritzki R.-P., Puls J., 2000, ARA&A, 38, 613
Kunze D., 1994, PhD thesis, Univ. Ludwing Maximilians
Kunze D., Kudritzki R.-P., Puls J., 1992, LNP, 401, 45
Kurucz R. L., 1991, BAAS, 23, 1047
Kurucz R. L., 1992, Rev. Mex. Astron. Astrofis., 23, 45
Lanz T., Hubeny I., 2003, ApJS, 146, 417
Leitherer C. et al., 1999, ApJS, 123, 3
Matthews T. A., Sandage A. R., 1963, ApJ, 138, 30
Martín-Hernández N. L., Vermeij R., Tielens A. G. G. M., van der Hulst J. M., Peeters E., 2002, A&A, 389, 286
Martins F., Schaerer D., Hillier D. J., 2005, A&A, 436, 1049
Meynet G., Maeder A., 2000, A&A, 361, 101
Meynet G., Maeder A., 2005, A&A, 429, 581
Mihalas D., Auer L. H., 1970, ApJ, 160, 1161
Mokiem M. R., Martín-Hernández N. L., Lenorzer A., de Koter A., Tielens A. G. G. M., 2004, A&A, 419, 319
Morisset C., 2004, ApJ, 601, 858
Morisset C., Schaerer D., Martín-Hernández N. L., Peeters E., Damour F., Baluteau J.-P., Cox P., Roelfsema P., 2002, A&A, 386, 558
Morisset C., Schaerer D., Bouret J.-C., Martins F., 2004, A&A, 415, 577
Najarro F., Kudritzki R. P., Cassinelli J. P., Stahl O., Hillier D. J., 1996, A&A, 306, 892
Najarro F., Hillier D., J., Puls J., Lanz T., Martins F., 2006, A&A, 456, 659
Oey M. S., Dopita M. A., Shields J. C., Smith R. C., 2000, ApJS, 128, 511
Osterbrock D. E., 1989, Phys. Today, 42, 123
Pauldrach A., Puls J., Kudritzki R. P., 1986, A&A, 164, 86
Pauldrach A. W. A., Hoffmann T. L., Lennon M., 2001, A&A, 375, 161
Puls J., 2008, in Bresolin F., Crowther P. A., Puls J., eds, Proc. IAU Symp. 250, Massive Stars as Cosmic Engenees. Cambridge Univ. Press, Cambridge
Puls J., Urbaneja M., A., Venero R., Repolust T., Springmann U., Jokuthy A., Mokiern M. R., 2005, A&A, 435, 669
Repolust T., Puls J., Herrero A., 2004, A&A, 415, 349
Repolust T., Puls J., Hanson M. M., Kudritzki R.-P., Mokiem M. R., 2005, A&A, 440, 261
Rubin R. H., Kunze D., Yamamoto T., 1995, in Adelmann S. J., Wiese W. L., eds, ASP Conf. Ser. Vol. 78, Astrophysical Applications of Powerful New Databases. Astron. Soc. Pac., San Francisco, p. 479
Rubin R. H. et al., 2007, MNRAS, 377, 1407
Santolaya-Rey A. E., Puls J., Herrero A., 1997, A&A, 323, 488
Schaerer D., 2000, in Alloin D., Olsen K., Galaz G., eds, ASP Conf. Ser. Vol. 221, Stars, Gas and Dust in Galaxies: Exploring the Links. Astron. Soc. Pac., San Francisco, p. 99
Schaller G., Schaerer D., Meynet G., Maeder A., 1992, A&AS, 96, 269
Sellmaier F. H., Yamamoto T., Pauldrach A. W. A., Rubin R. H., 1996, A&A, 305, L37
Simón-Díaz S., Herrero A., Esteban C., Najarro F., 2006, A&A, 448, 351
Stasińska G., 2004, in Esteban C., Garcia Lopez R. J., Herrero A., Sanchez F., eds, Cosmochemistry. Cambridge Univ. Press, Cambridge, p. 115
Stasińska G., 2007, 704, preprint (arXiv:0704.0348)
Stasińska G., Schaerer D., 1997, A&A, 322, 615
Smith L. J., Norris R. P. F., Crowther P. A., 2002, MNRAS, 337, 1309
Vacca W. D., Garmany C. D., Shull J. M., 1996, ApJ, 460, 914
Vilchez J. M., Pagel B. E. J., 1988, MNRAS, 231, 257
Villamariz M. R., Herrero A., 2000, A&A, 357, 597
Walborn N. R., 1972, AJ, 77, 312

APPENDIX A: GENERAL CHARACTERISTICS OF THE STELLAR ATMOSPHERE CODES

Below we summarize the main characteristics of the four stellar atmosphere codes considered in this study (we also refer to table 1 in Herrero 2007; Puls 2008) and give some notes on how the specific calculations of the models used here were performed.

Generally speaking, the four codes account for the NLTE and line-blanketing effects (although they also offer the possibility of calculating LTE and/or unblanketed models). TLUSTY is a plane-parallel, hydrostatic code, while the other three (FASTWIND, WM-*basic* and CMFGEN) belong to the family of model atmosphere codes so-called 'unified models' (Gabler et al. 1989), in which a spherically symmetric geometry, with a smooth transition between the photosphere and the wind, is considered.

A1 TLUSTY

TLUSTY is a plane-parallel hydrostatic code widely used nowadays. This code is aimed at the study of spectral lines formed in the photosphere, where velocities are small and the geometrical extension is negligible. The model atmosphere code is completed with SYNSPECT, a program for calculating the spectrum emerging from a given model atmosphere.

The basic concepts, equations and numerical methods used are described in Hubeny (1988). New developments included in subsequent versions are described in detail in Hubeny & Lanz (1992, 1995) and Hubeny, Hummer & Lanz (1994). One of the most important features of the new version of the program (v. 200) is that it

allows for a fully consistent, NLTE treatment of metal-line blanketing, either by means of Opacity Distribution Functions (ODF) or Opacity Sampling (OS).

The program is fully data oriented as far as the choice of atomic species, ions, energy levels, transitions and opacity sources is concerned (there are no default opacities built in). Note that to calculate realistic line-blanketed models with TLUSTY, all the above-mentioned atomic data need to be included explicitly in the calculations. This makes the model calculation to take about 4 h.

In order to construct realistic NLTE model atmospheres for O-type stars, Lanz & Hubeny (2003) included about 100 000 individual atomic levels of over 40 ions of H, He, C, N, O, Ne, Si, P, S, Fe and Ni in the calculation of their OSTAR2002 grid. The levels are grouped into about 900 NLTE superlevels. A total of 8000 lines of the light elements and about 2 million lines of Fe III–Fe VI and Ni III–Ni VI are accounted for in the calculations.

As commented in Section 2.1, we used three models from the OSTAR2002 grid for our study.

TLUSTY and SYNSPECT codes, the OSTAR2002 grid and all the atomic data files used in it can be downloaded from http://tlusty.gsfc. nasa.gov. There is also a very complete user's guide available.

A2 CMFGEN

CMFGEN was originally designed for the analysis of WR stars and luminous blue variables, with very dense winds. Subsequent developments of the code have allowed to also extend its application to O stars. Nowadays, CMFGEN can be used for detailed spectroscopic studies of hot stars from the (E)UV to the (F)IR ranges.

The approach driving this code is the inclusion of as many lines as possible in order to fully describe the effects of line blanketing, while minimizing the number of level populations to be explicitly solved [using the idea of superlevels, first pioneered by Anderson (1989)]. Radiative transfer is treated 'exactly' in this code (all lines are treated in comoving frame, even those from iron group elements), meaning that no opacity redistribution or sampling techniques are used. Consequently, CMFGEN is very time consuming (model calculation takes anything from 3–12 h, depending on the star and how close the initial guess is from the final solution).

Since CMFGEN was originally designed for the analysis of stars with very dense winds, the treatment of the photospheric density stratification is considered in an approximated way. At present, the velocity and density structures are not self-consistently computed but have to be given as input, either as input data or parametrized (see in Bouret et al. 2003, an example of how these structures are included in the code).

The CMFGEN models used in this study were kindly generated by F. Najarro and F. Martins. They used as initial guess for the model calculation previously calculated models with stellar parameters close to the required ones (see Table 1). Each model calculation took approximately 1 d.

A3 WM-basic

WM-*basic* aims mainly at the prediction of EUV/UV fluxes and profiles for hot luminous stars with homogeneous, stationary and spherically symmetric radiation-driven winds. In terms of the emergent spectrum calculation, in WM-*basic* models the bound–bound radiative rates are calculated in Sobolev approximation and the code does not include Stark broadening. Therefore, in WM-*basic*, the optical lines usually considered for the stellar parameter determination are not reliable for diagnostic purposes.

WM-*basic* provides a realistic stratification of the density and velocity, particularly in the transonic region, through the solution of the hydrodynamics produced by the scattering and absorption of Doppler shifted metal lines. The line contribution to the radiative acceleration is parametrized following the formulation by Castor, Abbott & Klein (1975) – CAK – (see also Pauldrach, Puls & Kudritzki 1986) that uses the concept of line-force multiplier and the force multiplier parameters (K, α and δ).

The authors have developed a fast numerical method which accounts for the blocking and blanketing influence of all metal lines in the entire subsonically and supersonically expanding atmosphere in a consistent manner (see Pauldrach et al. 2001). This method makes the computational time to be significantly reduced in comparison with e.g. CMFGEN calculations. To this end, detailed atomic models are implicitly considered by the code for all the important ions. These include 149 ionizations stages of 26 elements (H to Zn, apart from Li, Be, B and Sc), resulting in a total of 5000 levels. More than 30 000 bound–bound transitions for the NLTE calculations and more than 4 million lines for the line-force and blocking calculations are accounted for.

Our WM-*basic* models were generated with the easy-to-use Windows interface created by Adi Pauldrach for running the code.[9] The initial guess of the force multiplier parameters (K, α and δ) provided by WM-*basic* was slightly modified to produce the same $\dot{M}$ and v_∞ values than the ones used for FASTWIND and CMFGEN models (see Table 1). The models took ∼30–50 min to be converged.

A4 FASTWIND

FASTWIND (Santolaya-Rey et al. 1997; Puls et al. 2005) is optimized for the analysis of optical and IR spectra of OBA-type stars of all luminosity classes and wind strengths.

Among the main objectives that have guided the developers of FASTWIND since the initial version of the code a fast performance is the highest priority motivation. Since the first version, presented in Santolaya-Rey et al. (1997) to the latest one (last described by Puls et al. 2005), many improvements have been included in the code (the main ones are an approximate treatment of the line-blanketing/blocking effects and a consistent calculation of the temperature structure by means of the thermal balance of electrons).

The required computational efficiency is obtained by applying appropriate physical approximations to processes where high accuracy is not required (regarding the objective of the analysis: optical/IR lines). One of these approximations concerns the treatment of the opacity from metals (line blocking). We refer to Puls et al. (2005) for a detailed description of the method.

The code distinguishes between explicit elements, that are included in detail and can be synthesized later when solving the formal solution, and background elements producing the line blanketing and whose occupation numbers are calculated by solving the NLTE bound–bound rate equations in Sobolev approximation, in a similar way as WM-*basic* does. The calculation of the line-blanketing effects is hence independent on the elements considered explicitly.

Data from the background ions are taken from Pauldrach et al. (2001; WM-*basic*) and are provided in a fixed form.

Although FASTWIND is not aimed at predicting accurate ionizing spectral energy distributions (due to the simplified treatment of line blocking), we included it in our comparisons to test the reliability

---

[9] This is distributed as freeware and can be downloaded from the website: www.usm.uni-muenchen.de/people/adi/adi.html.

Table B1. Summary of nebular line ratios useful to test the predicted emergent ionizing SEDs.

Ionization edge	E_{ioniz} (eV)	λ (Å)	Ionic ratio	Line ratio	Optical range (Å)	IR range (μm)	Other lines
S⁺	23.3	531	$X(S^{2+})/X(S^+)$	[S III]/[S II]	[S III] 9531/[S II] 6716+30	–	[S III] 9069, 6312
Cl⁺	23.8	520	$X(Cl^{2+})/X(Cl^+)$	[Cl III]/[Cl II]	[Cl III] 5517+37/[Cl II] 8579	–	[Cl II] 9123, 6161
He⁰	24.6	504	He^+/H^+	He I/H I	He I λ 5876/Hβ^a	–	–
Ar⁺	27.6	448	$X(Ar^{2+})/X(Ar^+)$	[Ar III]/[Ar II]	–	[Ar III] 9.0/[Ar II] 7.0	[Ar III] 21.8
N⁺	29.6	419	$X(N^{2+})/X(N^+)$	[N III]/[N II]	–	[N III] 57.3/[N II] 121.7	–
S²⁺	34.8	356	$X(S^{3+})/X(S^{2+})$	[S IV]/[S III]	–	[S IV] 10.5/[S III] 18.7	[S III] 33.5
O⁺	35.1	353	$X(O^{2+})/X(O^+)$	[O III]/[O II]	[O III] 5007/[O II] 3726+29	–	[O III] 4959, 4363, [O II] 7320+30
Cl²⁺	39.6	312	$X(Cl^{3+})/X(Cl^{2+})$	[Cl IV]/[Cl III]	[Cl IV] 8048/[Cl III] 5517+37	–	–
Ne⁺	40.5	304	$X(Ne^{2+})/X(Ne^+)$	[Ne III]/[Ne II]	–	[Ne III] 15.6/[Ne II] 12.8	[Ne III] 36.0
Ar²⁺	40.7	302	$X(Ar^{3+})/X(Ar^{2+})$	[Ar IV]/[Ar III]	[Ar IV] 4711+40/[Ar III] 7751	–	[Ar IV] 7170, [Ar III] 7135
S³⁺	47.3	262	$X(S^{4+})/X(S^{3+})$	[S V]/[S IV]	–	–	–
N²⁺	47.5	261	$X(N^{3+})/X(N^{2+})$	[N IV]/[N III]	–	–	–

^a There are many other possible combinations of He I and H I lines available, both in the optical and IR.

of the approximate SED predicted by this code. FASTWIND models were calculated with version v8.5 of the code. Since we were only interested in the SED and the optical H and He lines, we considered H and He as the only explicit elements. This way we could generate FASTWIND models in only ~10–20 min.

APPENDIX B: NEBULAR LINE RATIOS BETTER SUITED TO TEST THE SHAPE OF THE STELLAR IONIZING SED

H II regions emit numerous H and He recombination lines in the optical, along with some forbidden lines from abundant metals. In addition, a rich spectrum of H recombination lines and fine structure lines is observed from the near- to far-IR (Ne, S, Ar: ~3–40 μm; C, N, O $\geq$40 μm). We refer to Stasińska (2007), who gives a list of useful lines from C, N, O, Ne, S, Cl and Ar ions and shows how to deal with them. Using appropriate nebular line ratios and taking into account the ideas presented above, one can impose constraints to test the predicted emergent ionizing SEDs.

Nebular line ratios involving a He I recombination line relative to a H I line (e.g. He I λ 5876/Hβ, in the optical) are important constraints. In an ionization bounded nebula, such a line ratio depends almost exclusively on the ratio $Q(He^0)/Q(H^0)$, provided that helium is not ionized in the entire nebula (which occurs if the effective temperature of the stellar ionizing source is $\geq$40 000 K).

Intensity ratios of lines from successive ions (X^{i+1} and X^i) of the same element can be used to constrain the ratio of ionic abundances and, as commented in Section 3.2.1, the number of stellar photons able to ionize X^i relative to the number of Lyman photons, $Q(X^i)/Q(H^0)$. In order to isolate the effect of the SEDs on the ionization structure from the effect on nebular temperature, it is better to use pairs of lines which have a similar dependence on the electron temperature, i.e. either pairs of recombination lines, or pairs of far-IR lines, or pairs of lines with similar excitation potentials (e.g. [S III] 9069/[S II] 6716+30 rather than [S III] 6312/[S II] 6716+30).

Table B1 gives the list of available nebular line ratios. For N, O, Ne, S, Cl and Ar, only nebular and fine-structure lines resulting from the lower energy levels are considered. In those cases, when various lines are available in the optical or IR ranges, the most intense ones are selected, though other possible lines are also indicated in the last column.

This paper has been typeset from a TEX/LATEX file prepared by the author.